A High-Order, Time Invariant, Linearized Model for Application to HHC/AFCS Interaction Studies

Rendy P. Cheng*
Mark B. Tischler†
Army/NASA Rotorcraft Division
Aeroflightdynamics Directorate (AMRDEC)
Ames Research Center, Moffett Field, CA 94035

Roberto Celi‡
Alfred Gessow Rotorcraft Center
Department of Aerospace Engineering
University of Maryland, College Park
College Park, MD 20742

Abstract

This paper describes a methodology for the extraction of a linear time invariant model from a nonlinear helicopter model, and followed by an examination of the interactions of the Higher Harmonic Control (HHC) and the Automatic Flight Control System (AFCS). This new method includes an embedded harmonic analyzer inside a linear time invariant model, which allows the periodicity of the helicopter response to be captured. The coupled high-order model provides the needed level of dynamic fidelity to permit an analysis and optimization of the AFCS and HHC loops. Results of this study indicate that the closed-loop HHC system has little influence on the AFCS or on the vehicle handling qualities, which indicates that the AFCS does not need modification to work with the HHC system. The results also show that the vibration response to maneuvers must be considered during the HHC design process, which leads to much higher required HHC loop crossover frequencies. This research also demonstrates that the transient vibration response during maneuvers can be reduced by optimizing the closed-loop higher harmonic control laws using conventional control system analyses.

Nomenclature

A_n	HHC n/rev amplitude, deg
AFCS	automatic flight control system
F	translational hub load, lb
HHC	higher harmonic control
J	cost function
LTI	linear time invariant
LTP	linear time periodic
M	rotational hub load, ft-lb
MCT	multiblade coordinate transformation
P	roll rate, rad/sec
Q	response weighting matrix
R	control weighting matrix
V	forward velocity, kt
Z	vibratory hub loads, lb, ft-lb
f	rotor equation
h	harmonic analyzer state vector
k	HHC feedback gain
x	helicopter state vector
u	helicopter control vector
Δz_{cg}	vertical displacement of the rotor hub, ft
δ_{lat}	piloted lateral command, in
μ	advance ratio
ω_c	crossover frequency, rad/sec
θ	HHC input harmonics
ζ	damping ratio

Superscript

$\dagger$	pseudo-inverse
T	transpose

Subscript

X	longitudinal axis
Y	lateral axis
Z	vertical axis
ave	average value
den	denominator
lat	lateral input
lon	longitudinal input
num	numerator
nc	cosine component of n/rev input/response
ns	sine component of n/rev input/response
0	reference case

*Research Scientist
†Flight Control Group Leader
‡Professor

Paper presented at the 59th Annual Forum of the American Helicopter Society, Phoenix, Arizona, May 6-8, 2003.

Introduction

Higher Harmonic Control (HHC) of a helicopter rotor has received increased attention over the last two decades, especially as a means of alleviating vibratory loads and reducing noise. Comprehensive reviews of the published literature on vibration reduction using HHC have been presented by Friedmann (Ref. 1) and Teves et al. (Ref. 2). To date, most of the studies have concentrated on the HHC algorithm, and they have not addressed the potential interactions between the HHC and the Automatic Flight Control System (AFCS), including any impact on handling qualities. The published literature reports results of flight tests, wind tunnel tests, and numerical simulations with either a closed-loop HHC system or a closed-loop AFCS, but not with both loops closed simultaneously.

Owing to the periodic nature of helicopters, HHC is a control system application that has developed without the benefit of standard control system analysis techniques. Without the use of these standard techniques, the application is placed at a relative disadvantage with respect to conventional control system designs. Although Floquet theory can be used to study such periodic systems, there are far more control system design theories and software tools that are available for linear time invariant systems than for periodic systems. Also, the entire portion of the Handling Qualities Specifications (ADS-33, Ref. 3) that addresses small perturbation maneuvers assumes that the linear model is time invariant. This exemplifies the need for time invariant linearized approximations that accurately model the coupled rotor-fuselage dynamics, including the higher harmonic response of the rotor. Such time invariant linearized approximation methods are not currently available and are a key focus of this paper.

Traditional linearization techniques lead to a Linear Time Periodic (LTP) system in the rotating frame. Typically, the HHC input is implemented in the rotating frame. If a Multiblade Coordinate Transformation (MCT) of the rotor equations is followed by averaging to eliminate time dependency, the averaging also eliminates all the higher harmonics both in the blade controls and in the rotor response. If the HHC input is introduced in the fixed frame after the averaging, the periodicity of the control inputs is preserved, and the HHC input will force this LTP system to respond in a n/rev fashion. The closed-loop stability of AFCS/HHC interaction can then be checked using the Floquet theory. This system, however, cannot produce n/rev vibration characteristics without the HHC inputs; therefore, the effects of the pilot's inputs on the vibration response cannot be correctly represented by this linear model.

The objective of the current study is to couple the flight dynamics and handling qualities disciplines to allow analysis of HHC and AFCS interaction. The specific objectives are:

1. Develop and validate a method for the extraction of a LTI-HHC models that includes the closed-loop HHC system.

2. Analyze the possibility of interactions between higher harmonic control and automatic flight control systems using the LTI-HHC model.

3. Optimize the performance of the closed-loop HHC system using conventional control system analyses.

Mathematical Model of the Helicopter

The mathematical model of the helicopter used in this study is similar to Sikorsky UH-60 Black Hawk. The model is based on a set of coupled nonlinear rotor-fuselage equations in first-order, state-space form, and the rigid-body dynamics of the helicopter are modeled using nonlinear Euler equations. The rotor model describes the dynamics of each blade with rigid-body coupled flap, lag, and first torsion mode degrees of freedom. Main rotor inflow is calculated using a three-state dynamic inflow model, which yields a linear inflow distribution over the rotor disk. For the tip loss, the outermost 3% of the rotor blade is assumed to generate profile drag but not lift. A one-state dynamic inflow model is used for the tail rotor. All the results presented in this paper were obtained from a coupled rotor-fuselage trim procedure simulating free flight conditions. The trim procedure enforces force and moment equilibrium about the body axes and periodicity of the rotor blade motion. Additional details of the mathematical model, including validation results, can be found in Refs. (4–6).

Although the mathematical model is limited to rigid flap-lag and first torsion blade dynamics, quasi-steady compressible aerodynamics, linear inflow, and a straight tip, this level of sophistication is adequate to capture the first-order effects, but it may not be sufficient for accurate quantitative predictions such as vibratory hub loads.

Effect of HHC Input on Traditional LTI Model

As stated earlier, traditional Linear Time Invariant (LTI) model extraction techniques do not capture the higher

harmonic nature of helicopter vibrations. Traditional linearization techniques consist of perturbing each state and control about an equilibrium position. Using this approach, the individual blade pitch is introduced in terms of the harmonics in the rotating frame. This method leads to systems of rotor equations containing periodic coefficients, which are represented in the rotating frame. The transformation from the rotating frame to the fixed frame is accomplished using a multi-blade coordinate transformation. To remove the time dependency, the linearized models are computed over one rotor revolution, with the equal rotor azimuth increments, and then averaged to obtain a LTI system in the fixed frame. As a consequence, this averaging eliminates the periodicity of the system and all the higher harmonics in both the controls and the rotor response.

Figure 1 shows the effects of a 3/rev HHC input on hub loads, as they would be predicted by a traditional LTI model obtained through a MCT and subsequent averaging. For comparison, the figure also contains the results of a nonlinear simulation using the model described in the previous section. The 3/rev HHC input used in this figure demonstrates its effect on the hub loads, and that it is not the proper HHC input for vibration reduction. Two key observations can be obtained from this figure. The first is that before the application of the 3/rev control, a steady vibration level is evident in the nonlinear model responses, but not in the linear model responses. The second is that after the 3/rev control is applied, the vibration level changes in the nonlinear model responses, but there is still no vibration in the linear model responses. Figure 2 shows the hub load time histories following a lateral doublet input (δ_{lat}) with HHC-off. Here, both linear and nonlinear models capture the mean hub load changes resulting from the lateral doublet input, but the results with the linear model do not include the higher harmonic responses that are seen in the nonlinear model simulation results. Clearly, this linear model cannot predict the higher harmonic behavior of hub loads.

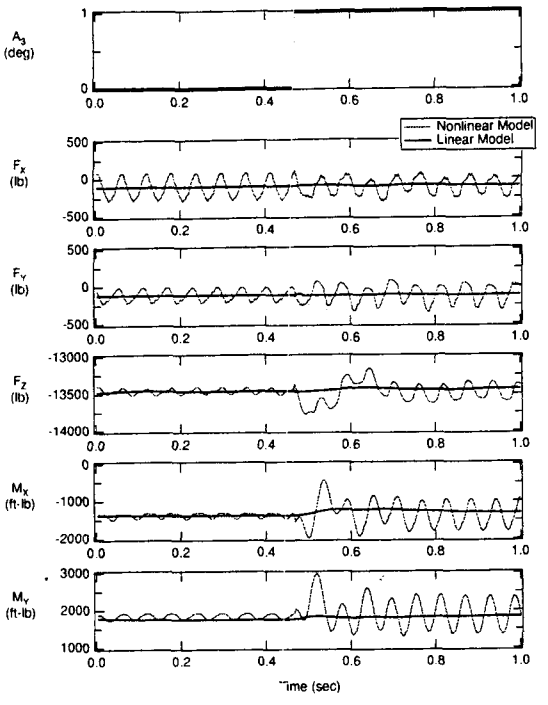

Figure 1: Hub loads comparison for the traditional linear model; HHC-on; V=120 kts (μ=0.28), Weight=14,000 lb.

Harmonic Analyzer

In wind tunnel and flight test (Ref. 7–10), a digital harmonic analyzer is used to extract hub load harmonics. A digital harmonic analyzer consists of applying a sample window, Fast Fourier Transform (FFT) and a lowpass filter to the data. When performing harmonic analysis with a physical system, it is necessary to truncate a long data stream from the measured signals to a finite size by applying a sample window. The sample window essentially behaves like a lowpass filter. As a result, the output of the harmonic analyzer contains little of the transient response, i.e., the application of windowing introduces a delay that masks the transient characteristics of the vibratory hub loads. For steady-state vibration suppression, this delay does not pose a problem.

Another method of extracting n/rev hub load harmonics is the analog harmonic analyzer (Ref. 11–13). It extracts the n/rev hub load harmonics using a bandpass filter. Initially, this appears to be a superior method; it directly provides a continuous sensor output without the impact on sampling time that is typically associated with FFTs in real-time applications. However, it has major drawbacks. This method requires a high order bandpass filter with narrow passband width to extract the steady-state vibration value. Moreover, the bandpass filter does not extract the n/rev hub load harmonics (cosine and sine components) directly; it only extracts the *amplitude* of the n/rev hub loads. Additional real-time processing is required to obtain the n/rev hub load harmonics. These requirements add a large time delay and equivalent phase lag to the system, usually much larger than the one caused by the sample window implemented in

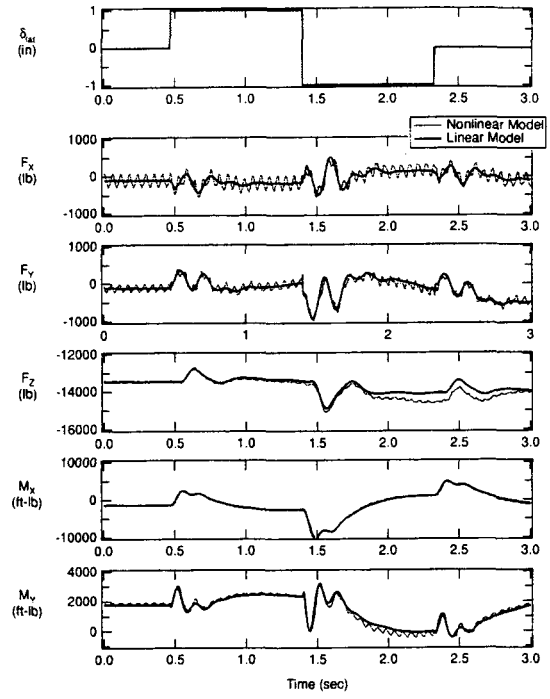

Figure 2: Hub loads comparison for the traditional linear model; lateral doublet input; HHC-off; V=120 kts (μ=0.28), Weight=14,000 lb.

the digital harmonic analyzer.

Once the hub load signal has been passed through the harmonic analyzer, the hub load harmonics are related to the HHC inputs using a transfer matrix controller (T-matrix) (Ref. 14). The HHC inputs are then computed and fed back to the rotor system for the vibration suppression as shown in Figure 3. There are two methods of capturing the periodic behavior of the helicopter as part of a Linear Time Invariant (LTI) model:

1. Add a LTI harmonic analyzer model in the feedback path of a LTI helicopter model

2. Generate a LTI helicopter model with an embedded harmonic analyzer

At a first glance, the first method appears to be the obvious choice, since it parallels the actual implementation of the real world case. If a LTI version of the harmonic analyzer is formulated, the HHC inputs will force the LTI helicopter model to respond at a 4/rev (4P) frequency for a 4-bladed helicopter. But, with the HHC feedback loops disengaged, the LTI helicopter model responses are limited to the 1/rev piloted input, and the LTI helicopter model does not exhibit any 4/rev behavior in either the rotor states or the hub loads. The effects of the AFCS on the vibratory hub loads (such as F_{X4c}/δ_{lat} open-loop frequency responses) cannot be correctly represented by this LTI helicopter model.

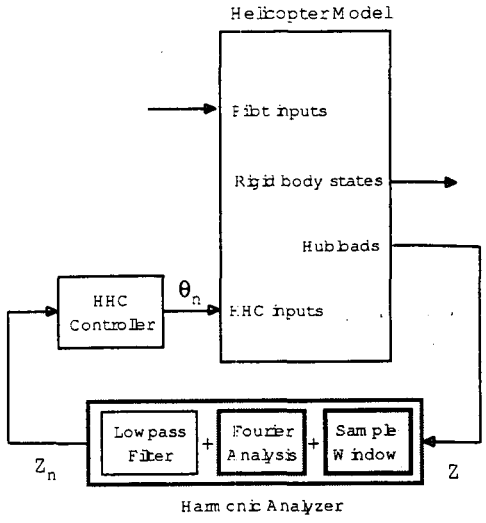

Figure 3: Closed-loop HHC vibration reduction scheme

Based on the limitations of the first method, the second method, which is to generate a LTI state-space model that preserves the periodic characteristics (referred as the LTI-HHC model) was selected for implementation. In this method, the periodic portion of the harmonic analyzer (Fourier analysis) is embedded within the LTI helicopter model. The embedded harmonic analyzer extracts the cosine and sine components of each rotor state. By embedding the harmonic analyzer within the LTI helicopter model and replacing the sample window with an equivalent lowpass filter, a closed-loop LTI-HHC system can be realized (Fig 4).

The state-space representation of the LTI-HHC model has the following form:

$$\begin{Bmatrix} \dot{\mathbf{x}} \\ \dot{\mathbf{h}}_{4P} \end{Bmatrix} = \begin{bmatrix} A_{11} & A_{12} \\ A_{21} & A_{22} \end{bmatrix} \begin{Bmatrix} \mathbf{x} \\ \mathbf{h}_{4P} \end{Bmatrix} + \begin{bmatrix} B_{11} & B_{12} \\ B_{21} & B_{22} \end{bmatrix} \begin{Bmatrix} \mathbf{u} \\ \mathbf{u}_{HHC} \end{Bmatrix} \quad (1)$$

$$\begin{Bmatrix} \mathbf{F}_{ave} \\ \mathbf{F}_{4P} \end{Bmatrix} = \begin{bmatrix} C_{11} & C_{12} \\ C_{21} & C_{22} \end{bmatrix} \begin{Bmatrix} \mathbf{x} \\ \mathbf{h}_{4P} \end{Bmatrix} + \begin{bmatrix} D_{11} & D_{12} \\ D_{21} & D_{22} \end{bmatrix} \begin{Bmatrix} \mathbf{u} \\ \mathbf{u}_{HHC} \end{Bmatrix} \quad (2)$$

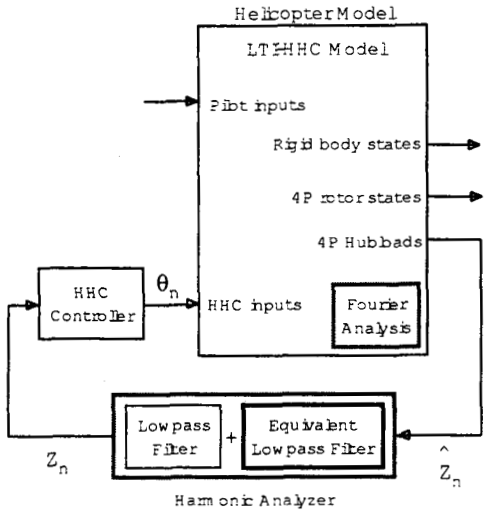

Figure 4: Analysis model of the closed-loop HHC vibration reduction scheme

where all the sub-matrices A_{ij} and B_{ij} of the state and control matrices, and the output equation matrices C_{ij} and D_{ij}, are time invariant. The $\mathbf{x}$ portion of the state vector contains the "averaged" components of the rotor and fuselage states, and $\mathbf{h}_{4P}$ contains the harmonic analyzer states. The $\mathbf{u}$ portion of the control vector contains the pilot and flight control system inputs, and $\mathbf{u}_{HHC}$ contains the HHC inputs. In the present study, $\mathbf{u}_{HHC}$ is assumed to be applied in the rotating system of a 4-bladed rotor, therefore it contains 3/, 4/, 5/rev cosine and sine harmonics, for a total of 6 inputs.

HHC Algorithm

The closed-loop HHC algorithm implemented is based on the fixed-gain T-matrix feedback controller:

$$Z_n = Z_{n-1} + T\,(\theta_n - \theta_{n-1}) \tag{3}$$

where Z is the response vector consisting of cosine and sine components of 4/rev vibratory hub loads (longitudinal, lateral, vertical hub shears plus pitching and rolling hub moments):

$$Z = f(Z_0, \theta) \tag{4}$$

and T is the Jacobian of f computed about a reference input, θ_0:

$$T = \left.\frac{\partial f}{\partial \theta}\right|_{\theta_0} \tag{5}$$

The input vector θ consists of the cosine and sine components of HHC inputs (3/rev, 4/rev, and 5/rev). Eq. (5) assumes that the response to HHC input is linear over the entire range of control application. For vibration suppression, the optimal control is obtained by minimizing the cost function J:

$$J = \frac{1}{2} Z_n^T Q\, Z_n + \frac{1}{2} \theta_n^T R\, \theta_n \tag{6}$$

where Q and R are the weighting matrices on the responses and controls:

$$Q = diag\{1,\ 1,\ 1,\ 1,\ 1,\ 1,\ q_7, \ldots,\ q_{10}\} \tag{7}$$

$$R = diag\{1,\ 1,\ 1,\ 1,\ 1,\ 1\} \tag{8}$$

and $q_7, \ldots, q_{10} = \frac{1}{\Delta z_{cg}^2}$ where Δz_{cg} is the vertical displacement of the rotor hub to the center of gravity of the helicopter. The choice of the weighting $\frac{1}{\Delta z_{cg}^2}$ transforms the moments to the equivalent forces. The optimal control is computed by setting the first derivative of the cost function of Eq. (6) to zero and solving for the optimal HHC input:

$$\frac{\partial J}{\partial \theta} = 0 \tag{9}$$

With this scheme, the HHC input is computed based on the current response vector:

$$\theta_n = \theta_{n-1} - T^{\dagger}\, Z_{n-1} \tag{10}$$

where the pseudo-inverse T-matrix is:

$$T^{\dagger} = (T^T Q\, T + R)^{-1} T^T Q \tag{11}$$

Equation (10) represents the HHC scheme applied in the discrete time domain. Its continuous time domain equivalent is simply an integrator, k/s, with a gain of k. Figures 5-7 illustrate the T-matrix vibration responses for 3, 4, and 5/rev inputs as numerically extracted from perturbing the nonlinear simulation with varying phase angles. The diamond symbol represents the baseline (HHC-off) 4/rev vibration responses from the nonlinear model, and their values are tabulated in Table 1. The open circles represent the vibration responses from the nonlinear model; the solid circles represent the extracted vibration responses from Eq. (3) with θ_n determined from Eq. (10). The numbers next to the symbols are the n/rev input phase angles. From these figures, the error resulting from the T-matrix approximation can be observed. For the 3/rev case (Figure 5), the T-matrix results match well with the nonlinear results. For the 4/rev and 5/rev cases, there are larger differences between the two methods. This difference is caused by the assumption that the response to the HHC input is linear over the entire range of control application.

Table 1: Baseline (HHC-off) Vibration Level

	4P Cos-Comp.	4P Sin-Comp.
F_X (lb)	151.6	87.8
F_Y (lb)	73.5	-61.3
F_Z (lb)	39.5	8.9
M_X (ft-lb)	40.1	62.6
M_Y (ft-lb)	80.0	30.2

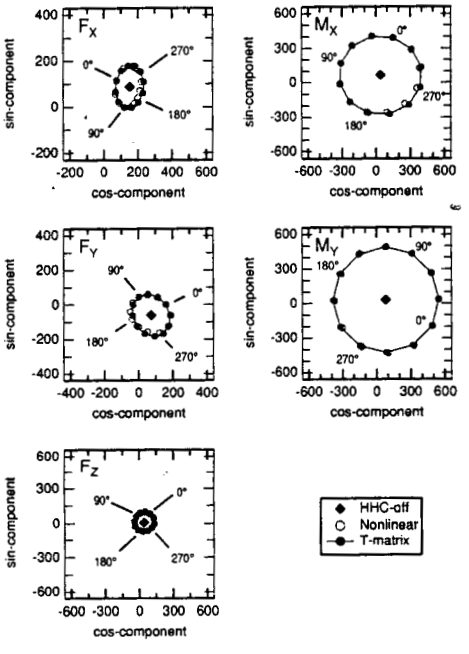

Figure 5: Extracted T-matrix response for an HHC input of $A_3 = 1°$; V=120 kts (μ=0.28), Weight=14,000 lb

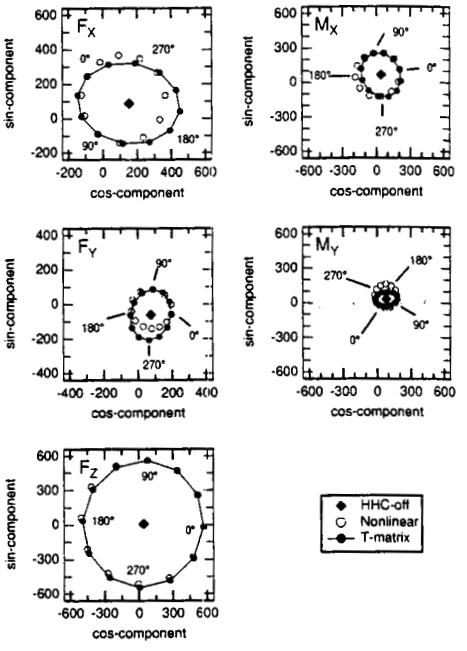

Figure 6: Extracted T-matrix response for an HHC input of $A_4 = 1°$; V=120 kts (μ=0.28), Weight=14,000 lb

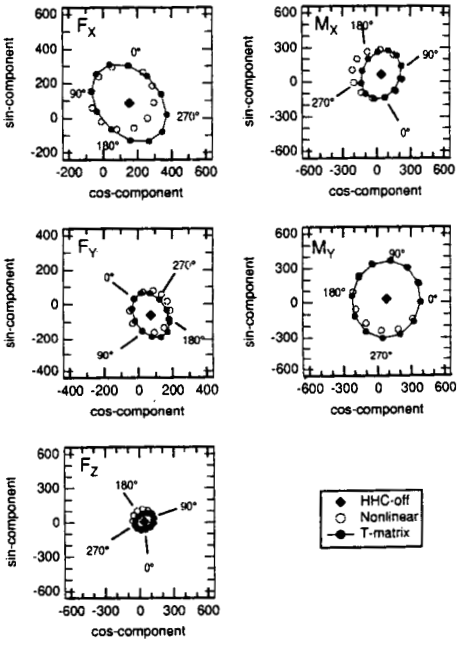

Figure 7: Extracted T-matrix response for an HHC input of $A_5 = 1°$; V=120 kts (μ=0.28), Weight=14,000 lb

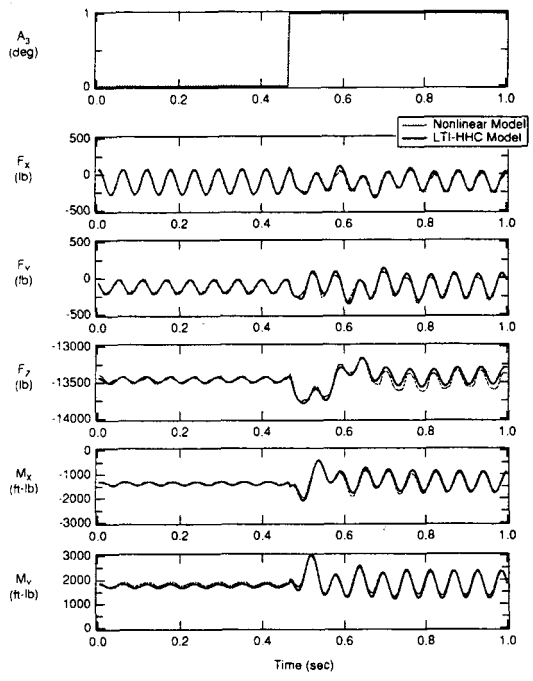

Figure 8: Validation of LTI-HHC model for HHC input; V=120 kts (μ=0.28), Weight=14,000 lb

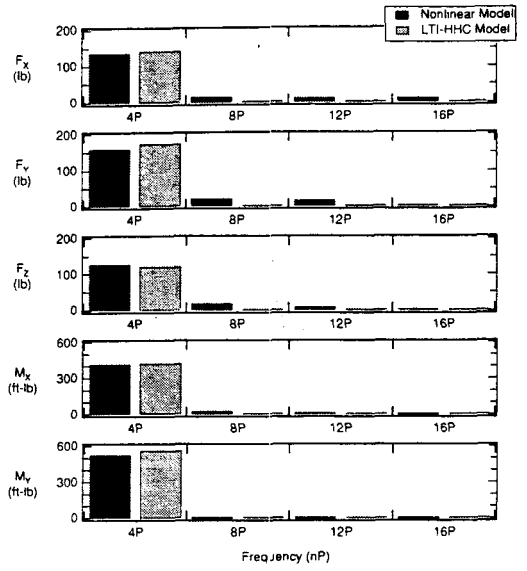

Figure 9: Hub load harmonic analysis; HHC on; V=120 kts (μ=0.28), Weight=14,000 lb

Linear Model Validations

The hub loads from the LTI-HHC model were validated against the nonlinear model results. Although the nonlinear model may not be sufficient for accurate quantitative predictions of vibratory hub loads, it has an adequate level of sophistication to capture the first-order effects. The flight configurations chosen for validation are hover, 40 kts, 80 kts, 120 kts, and 160 kts. The HHC input for these cases is a 3/rev input with amplitude of 1^o at the 0^o phase angle. Only the 120 kts (μ=0.28) case results are presented in this paper. Figure 8 shows that when the HHC input (A_3) is engaged, there is a little difference in hub load predictions between the LTI-HHC model and the nonlinear model.

The main difference in hub loads predictions is in the higher frequency contents (8/rev and 12/rev) of the translational hub loads (F_X, F_Y, F_Z). A spectral analysis of the hub loads was performed for both models with the HHC engaged. Figure 9 indicates that the nonlinear model has small 8/rev responses in all the translational hub loads, which are not modeled by this LTI-HHC model. This limitation can be overcome by including additional harmonic analyzer states in the LTI-HHC model. Similar conclusions can be drawn for the entire speed range. In terms of the 4/rev response, the LTI-HHC model is capable of producing results very close to those from the nonlinear model. The effects of piloted inputs on hub loads were also compared for both the nonlinear and LTI-HHC models (Figure 10). Overall, the LTI-HHC model is capable of predicting the nonlinear behavior in each axis throughout the entire speed range. Most of the differences appear in the vertical force (F_Z) and the pitching moment (M_Y) calculations.

Effect of a fixed HHC Input on Rigid-Body Dynamics

To understand the potential coupling between both control systems, an analysis was first performed with the HHC loops disengaged to determine whether a fixed HHC input had any direct effect on the rigid-body dynamics. First, the baseline (HHC-off) case of the LTI-HHC model was validated by comparing its frequency response against the flight test data. The frequency response of the nonlinear model, the LTI model and flight test are presented in Figure 11. The frequency response of the nonlinear model was obtained by performing frequency sweeps to extract the vehicle dynamics. The vehicle dynamics data were processed, and the frequency responses were identified using CIFER®(Ref. 15). All three cases agreed with each other in the frequency range

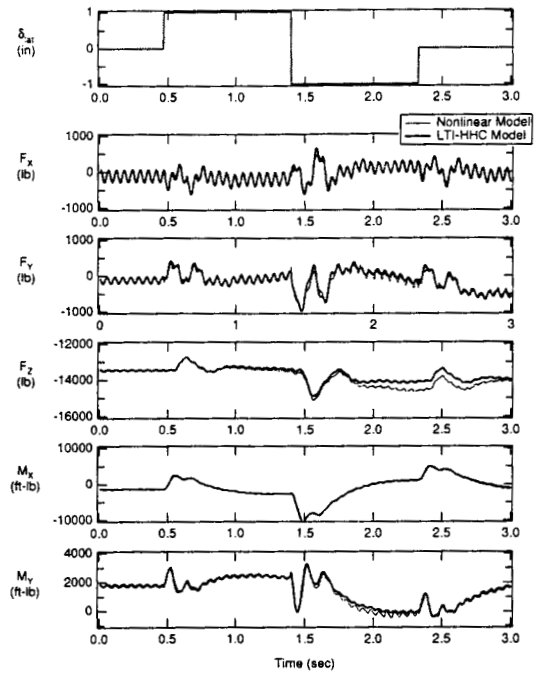

Figure 10: Validation of LTI-HHC model for lateral doublet input; HHC-off; V=120 kts (μ=0.28), Weight=14,000 lb

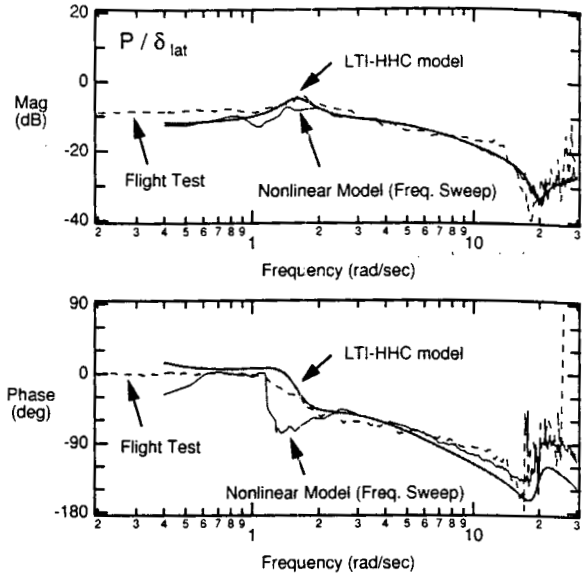

Figure 11: Linear model validation, baseline (HHC-off) case

of 2-20 rad/sec. There were some small disagreements in the frequency range of 1-2 rad/sec between the flight test result and the LTI-HHC model result.

Figure 12 shows the effect of a fixed HHC input on the rigid-body dynamics. The LTI-HHC model result was obtained with the HHC loop engaged. The nonlinear result was obtained by performing frequency sweeps on the nonlinear model with an optimum 3/rev input engaged. This optimum input was calculated based on an optimization procedure which minimized the hub shear. The figure indicates that the HHC input has no effect on the flight dynamics in the frequency range of interest for both models. The complete AFCS/HHC closed-loop analysis and control law optimization are performed in the next section.

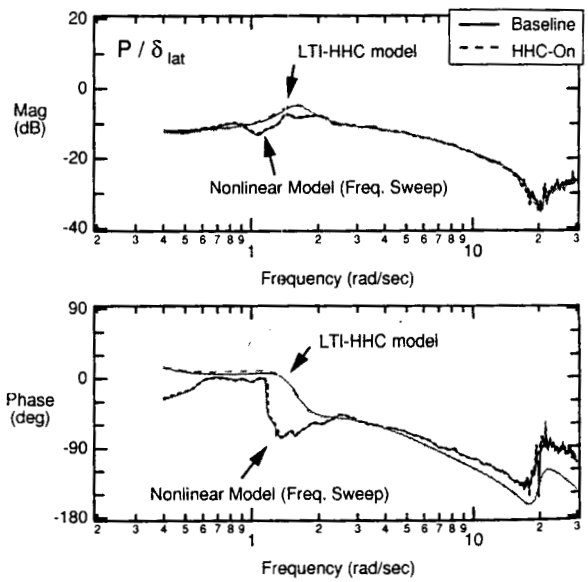

Figure 12: Effect of HHC input on rigid body dynamics

Interaction of Automatic Flight Control and Higher Harmonic Control

A SIMULINK® simulation of the integrated flight and higher harmonic control system was developed for analysis and optimization in the Control Designers Unified

Interface (CONDUIT®, Ref. 16). The key elements of the simulation are:

1. Higher-order linear airframe model (described above) that provides the flight mechanics and 4/rev vibration responses to both pilot and HHC inputs.
2. Automatic Flight Control System (AFCS) loops based on a simple proportional/integral/derivative (PID) controller in roll, pitch, and yaw to provide satisfactory attitude command/attitude hold handling-qualities.
3. Typical actuator/sensor filter dynamics
4. Higher harmonic control loops based on fixed T-matrix feedback.

First, CONDUIT was used to optimize the PID gains of the AFCS, with the HHC loops disengaged (Figure 13). The PID gains were tuned to achieve satisfactory handling-qualities, based on the Aeronautical Design Standard (ADS-33E, Ref. 3), and standard control-system design metrics:

(a) Crossover frequency (CrsMnG1, CrslnG1)

(b) Eigenvalue real part (EigLcG1)

(c) Stability margins (StbMgG1)

(d) Bandwidth (BnwRoF3)

(e) Step response damping ratio (OvsAtH1)

(f) Eigenvalue damping ratio (EigDgG1)

(g) Step response rise time (RisTmG1)

CONDUIT rapidly tuned the PID gains to achieve satisfactory (Level 1) requirements with minimum overdesign as shown in Fig 14. Each symbol represents the result for a particular loop and shows that all the responses lie in the light region (Level 1). For example, note that the roll bandwidth is 3 rad/sec (Fig. 14e), which meets ADS-33E. The PID gains of the roll and yaw loops yield bandwidths in excess of the requirement in order to meet some of the other specifications.

Next, the T-matrix HHC loops were engaged with a nominal gain of k=1 (same in all six loops), which corresponds to a crossover frequency, ω_c, of approximately 1 rad/sec (Fig. 15). The closing of the HHC loops had a negligible effect on the AFCS performance and overall handling-qualities, indicating the lack of dynamic coupling of HHC into flight control. Therefore, no re-tuning

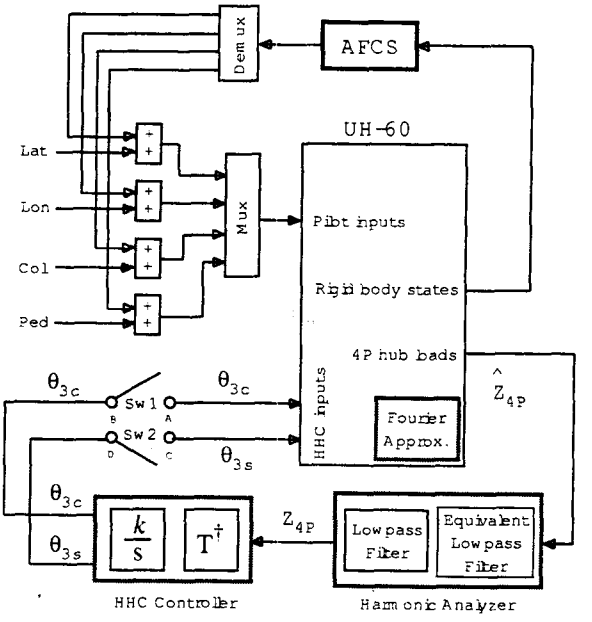

Figure 13: HHC/AFCS simulation diagram (Only the 3/rev inputs shown for clarity)

of the AFCS was needed for the combined AFCS/HHC system. The lack of interaction from HHC to flight control is consistent with the earlier system identification results obtained from the nonlinear simulation, which (Fig 12) showed no effect of an HHC frequency-sweep on the rigid-body dynamic response.

While the impact of HHC on handling-qualities is negligible, there is a significant vibration response to piloted inputs, both in the case of baseline (HHC-off) and with the nominal (k=1) HHC loop engaged. With the baseline case (HHC-off), Fig 16 shows that for a -50° roll maneuver (moderate), there is a maximum transient peak excitation of 150 lb addition to the trim vibration level in the F_{X4c} channel. This is roughly a doubling of the baseline trim vibration level (Table 1). With the nominal T-matrix controller (k=1) engaged, the maximum F_{X4c} vibration transient increases to 163 lb, which is 9% higher than the baseline case (HHC-off). In other words, with the nominal T-matrix controller engaged (k=1), the transient vibration response during maneuvering flight reaches similar levels to the trim condition with HHC-off. Nevertheless, the nominal T-matrix controller is able to reduce the transient load back to lower levels faster than baseline case after the 3-second point. Clearly, the vibration response to maneuvers must be considered in the design of the HHC system. Since, in this case, the fixed T-matrix

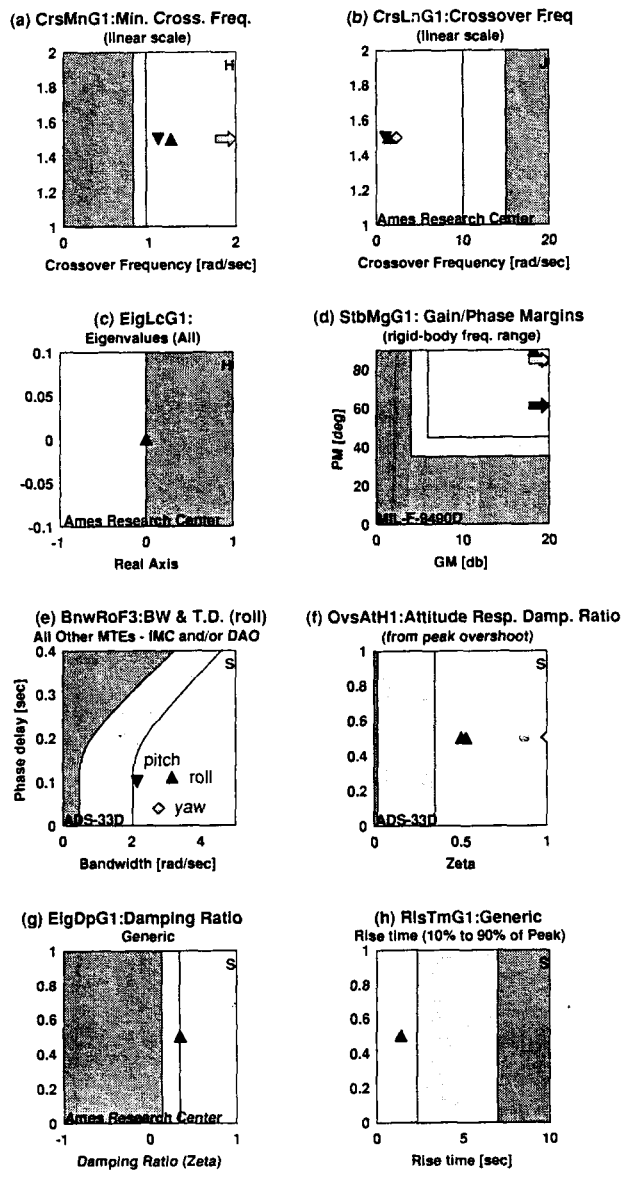

Figure 14: CONDUIT® handling-quality design specifications

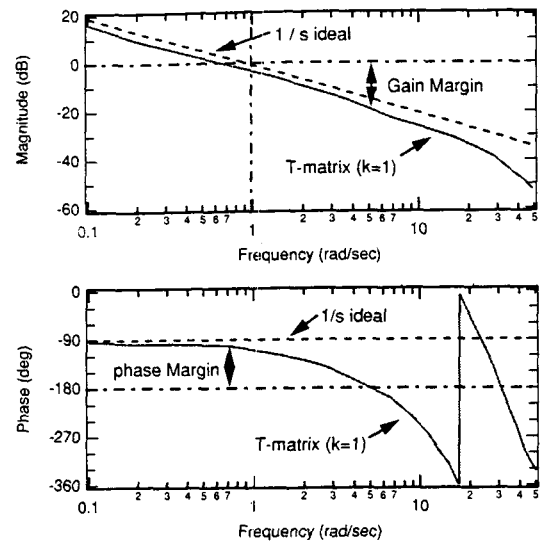

Figure 15: Broken-loop and disturbance responses of 3/rev input, T-matrix controller, nominal case (k=1)

is a close linear model of the nonlinear simulation dynamics, it represents a best case scenario for the performance with an adaptive T-matrix HHC system.

An analysis and optimization of the HHC loops (k=1) was conducted next in CONDUIT, with the AFCS gains fixed at their optimized values. The key specifications included in the analysis were HHC loop stability margins and vibration suppression performance. Gain and phase stability margins were determined for each of the six broken control loops (3/rev-sine, 3/rev-cosine, 4/rev-sine, 4/rev-cosine, 5/rev-sine, 5/rev-cosine). Figure 13 illustrates this HHC/AFCS simulation scheme. The broken control loop response is a method of studying loop stability. Using θ_{3c} broken-loop as an example, it is the response of θ_{3c} at point B (in Fig 13) with respect to the θ_{3c} input at point A while only switch 1 (Sw1 in Fig 13) is in the open position.

For steady-state vibration suppression, the helicopter vibration model (UH-60 in Figure 13) can be represented with a T-matrix which is a linear approximation of the vibration response to the HHC inputs at a steady-state condition. In other words, the T-matrix corresponds to the linear state-space model at DC gain (DC Gain is the ratio of the $output/input$ signal at the steady-state condition) to within the accuracy of the linear model extraction process. The nominal T-matrix controller (HHC Controller in Figure 13) is simply a k/s diagonal com-

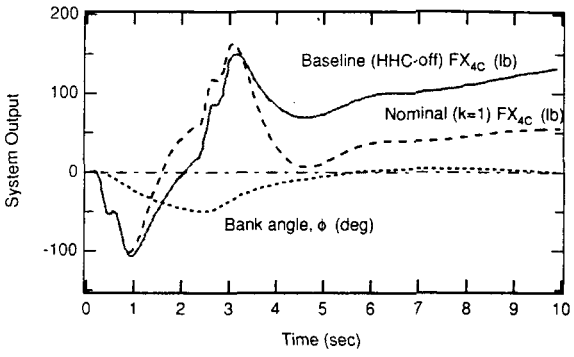

Figure 16: F_{X4c} vibration response in rolling maneuvering flight, T-matrix controller, nominal case (k=1)

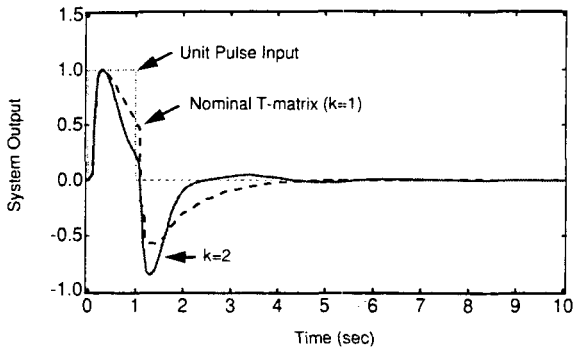

Figure 17: F_{X4c} unit pulse response; T-matrix controller, k=1 and 2

pensator multiplied by the pseudo-inverse ($T^{\dagger}$) of the steady-state response to HHC inputs. The broken-loop response matrix $(k/s)\ T^{\dagger}\ T$ will thus be a nearly diagonal matrix of k/s responses. This corresponds to single-input/single-output loop and without loop interactions (e.g., no response of the $3s$ loop to $3c$ transients). Assuming a nominal gain of k=1, this ideal approximation gives loop crossover frequencies of ω_c=1 rad/sec, 90° phase margin, and infinite gain margin in every loop as illustrated in Fig 15.

Next, the helicopter vibration model is replaced with the LTI-HHC model. The actual broken-loop response for the 3/rev-cosine loop shown in Fig 15 confirms that the k/s approximation is quite accurate for frequencies of up to about the 1 rad/sec crossover frequency. There is a gain offset associated with the deviation between the steady response of the nonlinear simulation (T) and the steady-state response of the linearized model. So, the actual crossover frequency is 0.72 rad/sec, with a phase margin and gain margin of 77° and 19 dB, respectively. For frequencies above 1 rad/sec, there is significant deviation from the 1/s ideal response, especially in phase due to the dynamics of the 4/rev vibration response relative to the simple steady-state approximation (T).

The response of the HHC loop for k=1 to a unit pulse input in vibration is shown in Fig 17 to be well damped. Increasing the HHC feedback gain (k=2), raises the broken-loop crossover frequency and raises the closed-loop HHC disturbance rejection bandwidth (Fig 18). There is an associated reduction in the closed-loop transient settling time, as was also concluded by Shin et al. (Ref. 17). But, there is also a magnification of the peak disturbance at frequencies above crossover (Fig 18) which is consistent with classical control theory,

Table 2: Vibration RMS with respect to piloted roll input; Normalized relative to maneuvering with HHC-off

	Nominal T-matrix (k=1)	Optimized Controller (Lead-Lag)
F_{X4c}	-4.1%	-41.8%
F_{X4s}	1.7%	-15.3%
F_{Y4c}	19.7%	-0.52%
F_{Y4s}	13.6%	-62.6%
Average	**7.7%**	**-30.0%**

and which shows up in the time-domain as well (Fig 17).

The performance of the HHC system in suppressing the vibration response to piloted inputs is reflected in the frequency-responses: F_{X4c}/δ_{lat}, F_{X4s}/δ_{lat}, F_{X4c}/δ_{lon}, etc. The RMS, determined from the integral under the frequency-response squared functions, is a useful measure of the vibration response to broadband piloted inputs for different HHC system designs. The spectral integration to determine the RMS is conducted up to a frequency of 3 rad/sec. The 3 rad/sec cut-off corresponds to the roll command bandwidth and is a good estimate of the maximum closed-loop piloting frequency. Finally, the RMS levels were normalized using the baseline (HHC-off) vibration RMS for the roll maneuver to show the relative improvement (or degradation) in vibration suppression by the HHC system.

For a nominal T-matrix controller, k=1, the average vibration in maneuvering flight is 7.7% above the baseline case (Table 2). This matches the time response comparison of Fig 16, and it shows again that the nominal T-matrix controller is ineffective for vibration suppression during maneuvers. Analyses with CONDUIT show

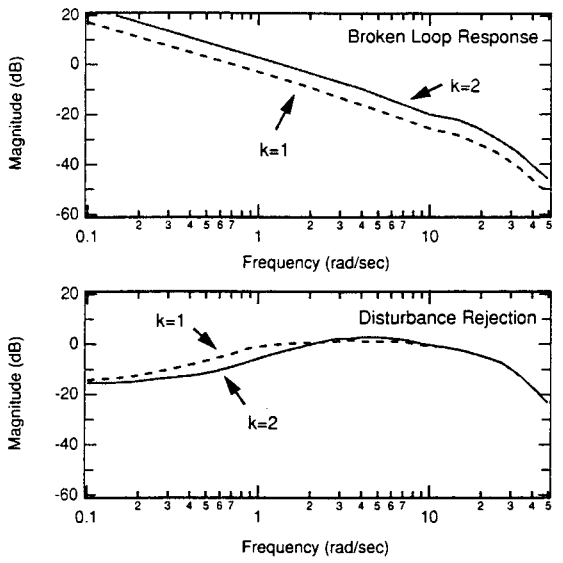

Figure 18: Broken-loop response of 3/rev input; T-matrix controller, k=1 and 2

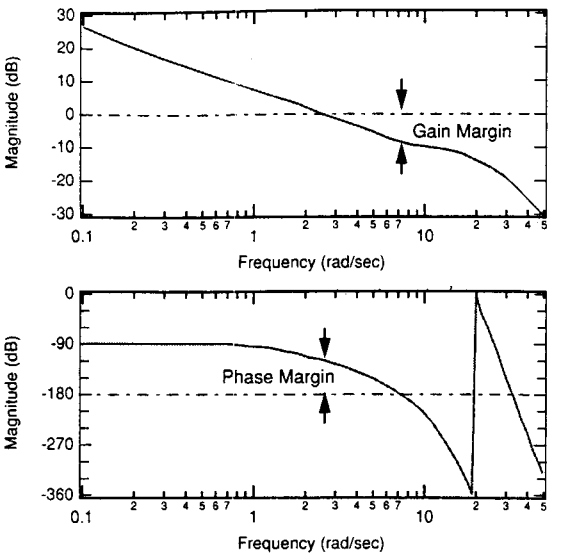

Figure 19: Broken-loop response of 3/rev input; optimized HHC system

that an improvement in the suppression of vibration transients during the roll maneuever input can only achieved by increasing the HHC crossover frequency to a value that is close to the 3 rad/sec piloted bandwidth. At this increased crossover frequency, the use of the steady-state (T) approximation is unacceptable for controller optimization and analysis (Fig 15), and the complete dynamic model developed earlier is required. Further, the simple k/s controller architecture must be augmented with the addition of a 2nd-order lead-lag compensation in each loop to achieve the needed stability margins. The HHC feedback controller now takes the form:

$$H(s) = \left(\frac{k}{s}\right)\left(\frac{\omega_{den}^2}{\omega_{num}^2}\right)\frac{[s^2 + 2\zeta_{num}\omega_{num}s + \omega_{num}^2]}{[s^2 + 2\zeta_{den}\omega_{den}s + \omega_{den}^2]} \quad (12)$$

Each HHC control loop contains 5 design parameters, and the same controller is used for the cosine and sine loops of a particular harmonic. Thus, for the three harmonics (6 loops), there are 15 HHC feedback parameters in total. As an illustration, CONDUIT was used to tune these parameters to minimize the sum of the normalized vibration RMS values for the four in-plane shears to a lateral input (F_{X4c}/δ_{lat}, F_{X4s}/δ_{lat}, F_{Y4c}/δ_{lat}, F_{Y4s}/δ_{lat}). The optimized results are presented in Table 2. The RMS vibration shears are reduced by 30% compared to the baseline (HHC-off) case and 35% compared to the nominal T-matrix controller (k=1) case. This is achieved by increasing the crossover frequencies to their maximum values (e.g., $\omega_c = 2.8$ rad/sec in the 3/rev loops) while still maintaining adequate stability margins (Fig 19).

The transient response of the optimized controller is compared to the baseline case in Fig 20 for the roll maneuver. The peak vibration is now 103 lb, or 31% below the baseline result, which again tracks the frequency-domain results of Table 2 closely. We can clearly see that the optimized controller has achieved performance superior to that of the baseline (HHC-off) and nominal T-matrix controller cases.

Conclusions

This paper illustrates a new methodology for the derivation of linearized, time invariant, state-space models of a helicopter, and uses this new model to study the interactions of HHC and AFCS. The LTI-HHC model, developed herein, captures the periodic characteristics of the helicopter by embedding the Fourier analysis of the harmonic analyzer within the plant model. The sample window within the harmonic analyzer is modeled using a simple lowpass filter and implemented in the HHC feedback path. Using this new analysis, the hub loads of the LTI-HHC model match the hub loads of the nonlinear

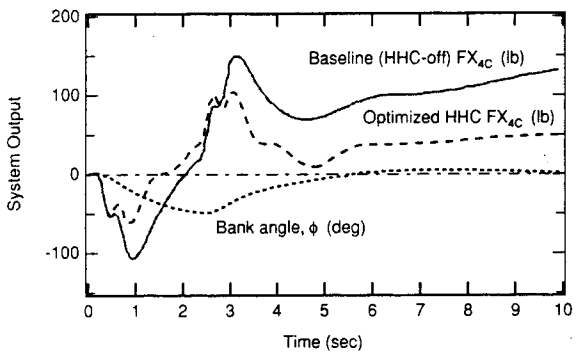

Figure 20: F_{X4c} vibration response in rolling maneuvering flight; optimized HHC system

model well for both HHC inputs and piloted inputs. This is an important result, since the traditional linearization method with averaging removes the periodicity of the response and, therefore, cannot be used to model rotor vibrations. One limitation of the LTI-HHC model described in this paper is that it can model only the 4/rev components of the harmonic analyzer states and not the higher frequency content (8/rev and 12/rev, etc.) of the nonlinear model. This limitation can be overcome, however, by including additional harmonic analyzer states in the LTI-HHC model. The LTI-HHC model was integrated with the flight and higher harmonic control system in SIMULINK®, and a complete AFCS/HHC loop analysis and control law optimization were performed in CONDUIT®.

The main conclusions of the present study are:

1. The closed-loop HHC system has little influence on flight control/handling-qualities.

2. Vibration response to maneuver inputs must be considered as part of the HHC system design process, and it will lead to much higher required loop crossover frequencies.

3. The nominal T-matrix controller (typical controller gain of k=1) does not provide additional vibration benefit over the baseline (HHC-off) case in a maneuvering flight.

4. Increasing the T-matrix controller feedback gain (k=2) reduces the closed-loop transient settling time, but it increases the magnitude of the peak disturbance at frequencies above crossover frequency.

5. For the same maneuvering flight, the optimized HHC system reduces vibratory shears by 30% compared to the baseline case and 35% compared to nominal T-matrix controller case.

References

(1) Friedmann, P. P., and Millot, T. A., "Vibration Reduction in Rotorcraft Using Active Control: A Comparison of Various Approaches," *Journal of Guidance, Control, and Dynamics*, Vol. 18, (4), July-August 1995.

(2) Teves, D., Niesl, G., Blaas, A., and Jacklin, S., "The Role of Active Control in Future Rotorcraft," 21st European Rotorcraft Forum, Saint Petersburg, Russia, September 1995.

(3) Anon., "Handling Qualities Requirements for Military Rotorcraft," Aeronautical Design Standard-33 (ADS-33E-PRF), US Army Aviation and Missile Command, March 21, 2000.

(4) Kim, F.D., Celi, R., and Tischler, M.B., "High Order State Space Simulation Models of Helicopter Flight Mechanics," *Journal of the American Helicopter Society*, Vol. 38, (2), October 1993.

(5) Kim, F.D., Celi, R., and Tischler, M.B., "Forward Flight Trim Calculation and Frequency Response Validation of a High-Order Helicopter Simulation Model," *Journal of Aircraft*, Vol. 30, (6), November-December 1993.

(6) Theodore, C., and Celi, R., "Helicopter Flight Dynamic Simulation with Refined Aerodynamic and Flexible Blade Modeling," *Journal of Aircraft*, Vol. 39, No. 4, July-August 2002.

(7) Jacklin, S. A., Nguyen, K. Q., Blaas, A., Richter, P., "Full-Scale Wind Tunnel Test of a Helicopter Individual Blade Control System," Proceedings of the 50th Annual Forum of the American Helicopter Society, May 1994.

(8) Arnold, U. T. P., Strecker, G., "Certification, Ground and Flight Testing of an Experimental IBC System for the CH-53G Helicopter," Proceedings of the 58th Annual Forum of the American Helicopter Society, June 2002.

(9) Nguyen, K. Q., Chopra, I., "Application of Higher Harmonic Control to Rotor Operating at High

Speed and Thrust," *Journal of the American Helicopter Society*, Vol. 35, (3), July 1990.

(10) Nguyen, K. Q., Betzina, M., Kitaplioglu, C.,"Full-Scale Demonstration of Higher Harmonic Control for Noise and Vibration Reduction on the XV-15 Rotor," Proceedings of the 56th Annual Forum of the American Helicopter Society, May 2000.

(11) Wood, E. R., Powers, R. W., Cline, J. H., "On Developing and Flight Testing a Higher Harmonic Control System," *Journal of the American Helicopter Society*, Vol. 30, (1), 1985.

(12) Hammond, C. E., "Wind Tunnel Results Showing Rotor Vibratory Loads Reduction Using Higher Harmonic Blade Pitch," *Journal of the American Helicopter Society*, Vol. 28, (1), 1983.

(13) Shaw, J., Albion, N., Hanker, E. J., Jr., and Teal, R. S., "Higher Harmonic Control: Wind Tunnel Demonstration of Fully Effective Vibratory Hub Force Suppression," *Journal of the American Helicopter Society*, Vol. 34, (1), 1989.

(14) Nguyen, K. Q., and Chopra, I., "Effects of Higher Harmonic Control on Rotor Performance and Control Loads," *Journal of Aircraft*, Vol. 29, (3), May-June 1992.

(15) Tischler, M.B. , and Cauffman, M.G., "Frequency-Response Method for Rotorcraft System Identification: Flight Applications to BO-105 Coupled Rotor/Fuselage Dynamics," *Journal of the American Helicopter Society*, Vol 37, No 3, July 1992.

(16) Tischler, M. B., et al, "A Multidisciplinary Flight Control Development Environment and Its Application to a Helicopter," *IEEE Control Systems Magazine*, Vol. 19, No. 4, August 1999.

(17) Shin, S. J., Cesnik, C. E. S., and Hall, S. R., "Control of Integral Twist-Actuated Helicopter Blades for Vibration Reduction," Proceedings of the 58th Annual Forum of the American Helicopter Society, June 2002.